Materials & Design 223 (2022) 111243

Contents lists available at ScienceDirect

Materials & Design

journal homepage: www.elsevier.com/locate/matdes

Formation, evolution and characterization of nanoporous structures on the Ti6Al4V surface induced by nanosecond pulse laser irradiation

Chao Wang [a], Hu Huang [a,*], Zhiyu Zhang [b], Lin Zhang [c], Jiwang Yan [c], Luquan Ren [d]

[a] Key Laboratory of CNC Equipment Reliability, Ministry of Education, School of Mechanical and Aerospace Engineering, Jilin University, Changchun, Jilin 130022, China
[b] Key Laboratory of Optical System Advanced Manufacturing Technology, Changchun Institute of Optics, Fine Mechanics and Physics, Chinese Academy of Sciences, Changchun, China
[c] Department of Mechanical Engineering, Faculty of Science and Technology, Keio University, Yokohama 223-8522, Japan
[d] Key Laboratory of Bionic Engineering Ministry of Education, Jilin University, Changchun, Jilin 130022, China

HIGHLIGHTS

- Nanaoporous structures were fabricated on the Ti6Al4V surface by nanosecond pulse laser irradiation.
- Their porosity can be easily tuned by changing the laser parameters.
- The surface with nanoporous structures exhibited similar surface hardness but superior tribological performance.
- The formed nanoporous structures could tune the surface wettability.

GRAPHICAL ABSTRACT

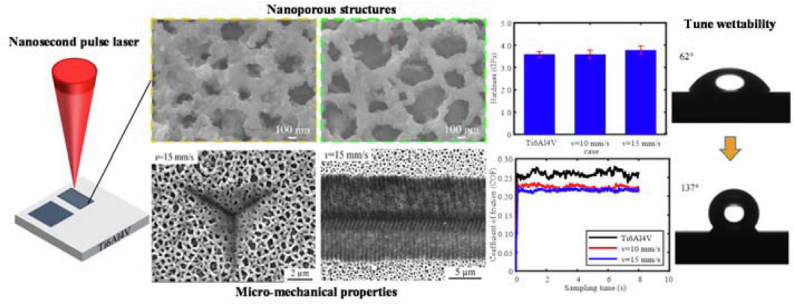

ARTICLE INFO

Article history:
Received 17 June 2022
Revised 13 September 2022
Accepted 6 October 2022
Available online 7 October 2022

Keywords:
Nanosecond pulse laser
Nanoporous structures
Surface hardness
Tribological performance
Wettability

ABSTRACT

Manipulating materials at nanoscale is challenging but rewarding. Nanostructures exhibit some unique properties distinguished from macroscopic bulk materials, so fabrication of nanostructures on the material surface is beneficial to broaden their functional applications. In this study, by nanosecond pulse laser irradiation in nitrogen atmosphere, it was found that unique nanoporous structures could be formed on the Ti6Al4V surface. The effects of laser parameters including the laser power, overlap rate, scanning speed, and repetition frequency on the formation and evolution of the nanoporous structures were systematically investigated. By changing the laser parameters, the nanoporous structures with various porosities could be easily achieved on the Ti6Al4V surface. According to the structural evolution and chemical composition, the formation mechanism of the nanoporous structures was discussed. Furthermore, by characterizing the micro-mechanical properties and wettability, it was found that the surface with nanoporous structures exhibited similar surface hardness but improved tribological performances compared to the original Ti6Al4V surface, and the surface wettability could be tuned. This study provides a simple method for fabricating nanoporous structures on the Ti6Al4V surface, which would broaden its functional applications.

1. Introduction

Due to the unique size effects [1,2], nanomaterials exhibit unconventional properties distinguished from macroscopic bulk materials, such as ultrahigh-specific surface area, novel optical, thermal, and electromagnetic properties. Therefore, manipulating

* Corresponding author.
E-mail address: huanghu@jlu.edu.cn (H. Huang).

https://doi.org/10.1016/j.matdes.2022.111243
0264-1275/

Table 1
The experimental conditions.

Laser parameter	Value
Laser power P (W)	1.35, 1.48, 1.61, 1.75
Laser scanning speed v (mm/s)	5, 10, 15
Laser overlap rate between two adjacent scanning lines r	88.3 %, 76.6 %, 64.3 %
Laser repetition frequency f (kHz)	500, 600, 700, 800, 900

materials at the nanoscale has always attracted considerable attention [3,4]. As a member of the nanomaterial family, nanoporous materials have shown promising application prospects in catalyst carriers [5], signal sensing [6], electromagnetic shielding [7], energy storage [8], and lightweight design [9]. For example, due to the ultrahigh-specific surface area, nanoporous materials can provide more catalytic sites and achieve better catalytic effects [10]. Besides, it also breaks through the limitations in energy storage for some traditional materials such as fuel cells and lithium batteries [11]. Many approaches have been developed for fabricating the nanoporous structures on various material surfaces [12–14]. While for the metal materials, the commonly employed method for preparing the nanoporous structures is dealloying [15–17], which is based on the principle of electrochemical corrosion. However, this method is limited by the electrochemical characteristics of metal samples as well as the pollutants generated during the processing. Therefore, it is urgently desired to explore new methods for fabricating the nanoporous structures on metal surfaces.

Taking advantages of high specific strength, excellent corrosion resistance, and outstanding biocompatibility, titanium and its alloys are widely applied in orthopedics and dental implants [18]. Some previous studies [19,20] have shown that porous titanium is beneficial to the proliferation and differentiation of bone cells, promoting the combination of bone cells and implants. For example, Su et al. reported that the nanoporous structures on the Ti6Al4V surface improved the adhesion of osteogenic cells [21]. Xia et al. systematically studied the effects of nanoporous structures with different pore sizes on the diffusion and differentiation of bone marrow-derived stem cells [22]. Besides, Ramis et al. demonstrated that the nanoporous structures could improve the integration of soft tissues around the implant [23]. Accordingly, the fabrication of nanoporous structures on titanium alloys is of great importance. Apart from dealloying, some other strategies such as additive manufacturing [24,25], anodization [26], and hydrothermal reaction [27] have also been used to fabricate the nanoporous structures on titanium alloys, but they still face the drawbacks of being time-consuming and expensive. Therefore, it is quite meaningful to develop an alternative method for the fabrication of nanoporous structures on titanium alloys.

Laser processing, as a flexible, efficient, and environmentally friendly method, without the requirement for stabilizers and other chemicals, has shown potential application in the fabrication of micro/nano-structures [28]. By laser-material interaction, it is easy to generate some micro/nano-structures such as nanoparticles [29,30], ripples [31], and other structures [32]. However, few studies have focused on the fabrication of nanoporous structures on titanium alloys by laser processing alone. In this study, by nanosecond pulse laser irradiation in nitrogen atmosphere, nanoporous structures were successfully fabricated on the Ti6Al4V surface. The effects of laser parameters on the formation and evolution of nanoporous structures were investigated in detail, followed by characterizing their micro-mechanical properties and wettability.

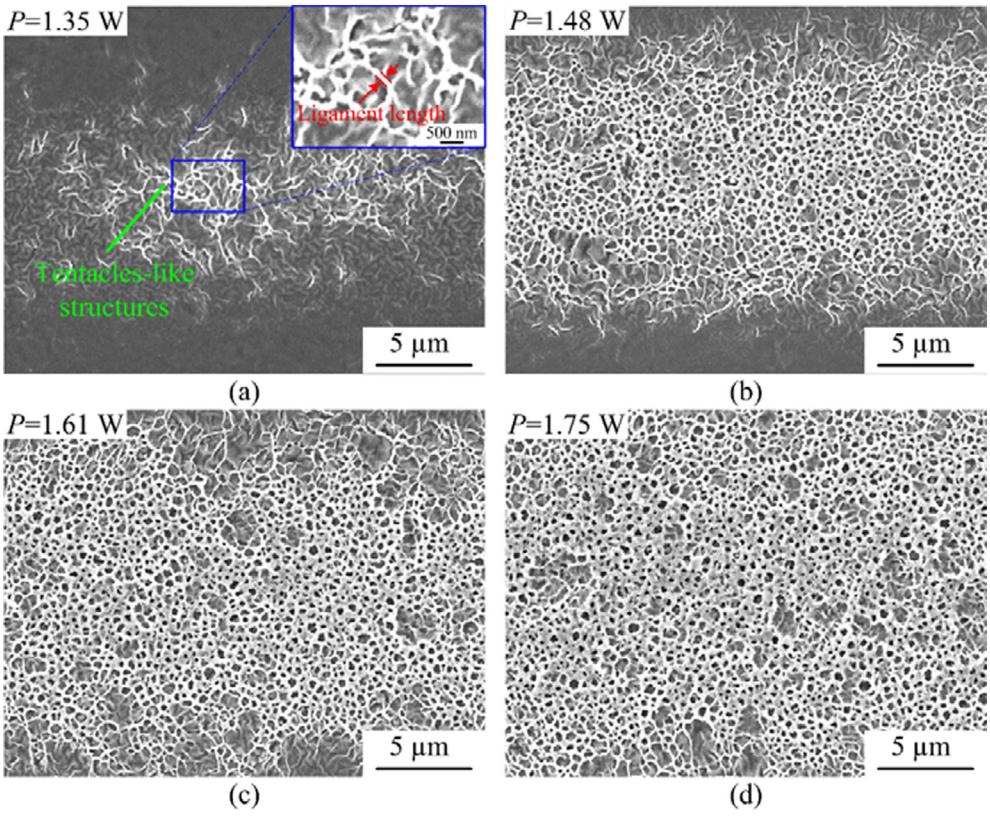

Fig. 1. SEM morphologies of the single-line scanned regions obtained under various laser powers (v = 10 mm/s, f = 700 kHz): (a) 1.35 W, (b) 1.48 W, (c) 1.61 W, and (d) 1.75 W.

2. Materials and experiments

The commercial Ti6Al4V samples with a dimension of 40 mm × 40 mm × 3 mm were used in the experiments. To obtain a mirror-like surface, the samples were ground by using 400, 800, 1200, 1500, and 2000 sandpapers and then polished in sequence. The as-prepared samples were irradiated by a fiber pulse laser system (SP-050P-A-EP-Z-F-Y, SPI, UK) with a pulse width of 7 ns and central wavelength of 1064 nm. The laser beam has a Gaussian profile (TEM_{00} mode, $M^2 < 1.6$) with a focused spot diameter of ~ 42 μm. To obtain a uniform surface structure, the "S" scanning path was employed. The experiments were performed in pure nitrogen atmosphere with a pressure of 0.05 MPa. To investigate the evolution of laser-induced surface structure, various laser powers, overlap rates, scanning speeds, and repetition frequencies were employed, as listed in Table 1. The overlap rates of 88.3 %, 76.6 %, and 64.3 % correspond to the intervals of 5, 10, and 15 μm between two adjacent scanning lines, respectively.

The laser irradiated surfaces were observed by using a tungsten filament scanning electron microscope (SEM, JSM-IT500A, JEOL, Japan), field emission scanning electron microscope (SEM, JSM-7900F, JEOL, Japan), and the laser scanning confocal microscope (LSCM, OLS4100, Olympus, Japan). The ImageJ software was used to analyze the pore size and porosity of the laser irradiated surface. The element distribution of the laser irradiated surface was detected by using an energy dispersive X-ray spectroscopy (EDS, EX-74600U4L2Q, JEOL, Japan). An X-ray diffractometer (XRD, D8 Discover, Bruker, Germany) was employed to characterize the crystal phases of the Ti6Al4V and laser irradiated surfaces. The surface hardness of the Ti6Al4V and laser irradiated surfaces was measured via a nanoindentation (DUH-211S, SHIMADZU, Japan) equipped with a pyramidal diamond indenter with an angle of 115° between the ridge and face (TOKYO DIAMOND Tools MFG. Co., Ltd., Japan). The maximum indentation load and loading rate were 100 mN and 10 mN/s respectively. The scratch tests were performed by using a self-made piezoelectric driven scratch instru-

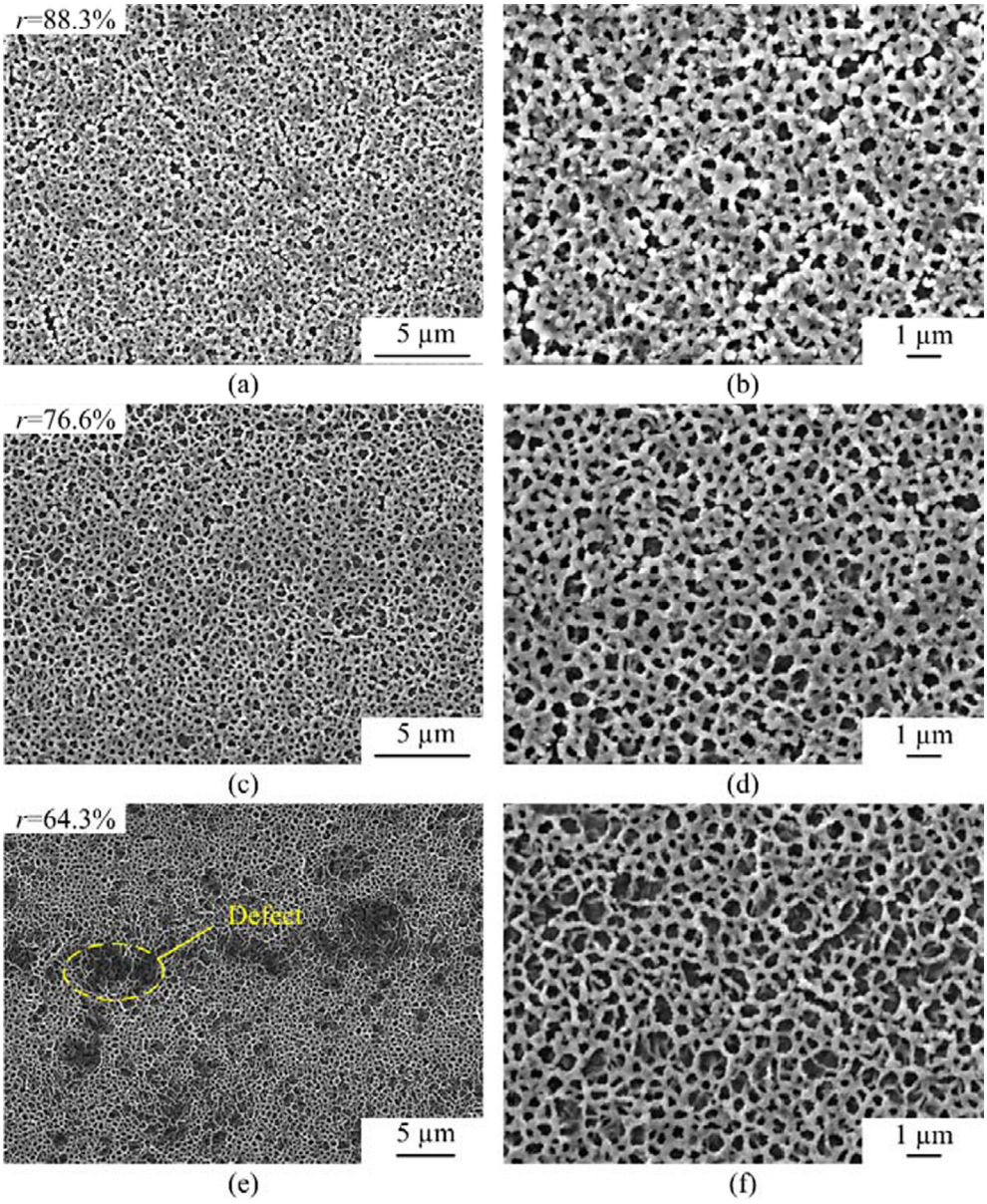

Fig. 2. SEM morphologies of the multi-line scanned regions obtained under various overlap rates (P = 1.48 W, v = 10 mm/s, f = 700 kHz): (a) r = 88.3 %, (c) r = 76.6 %, and (e) r = 64.3 %. (b), (d), and (f) are the local enlarged images of Fig. 2(a), (c), and (e), respectively.

ment equipped with a diamond Vickers indenter. The scratching load was 100 mN and the scratching speed was 20 μm/s. After laser irradiation, the samples were immersed into 1H,1H,2H,2H-Perfluor ooctyltriethoxysilane-ethanol solution with a concentration of 1 wt% for 1 h, followed by drying at room temperature for 30 min. Before and after chemical modification, the wettability of the polished and irradiated surfaces was evaluated by measuring the contact angle using a contact angle measuring instrument (OAS60, NBSI, China).

3. Results and discussion

3.1. Formation and evolution of the nanoporous structures

Fig. 1 shows the SEM morphologies of single-line scanned regions obtained under various laser powers. The employed laser scanning speed and repetition frequency are 10 mm/s and 700 kHz, respectively. As shown in Fig. 1(a), when the laser power is 1.35 W, some irregular tentacles-like structures appear in the laser irradiated region of the Ti6Al4V surface. From the enlarged image, the ligament length of the generated tentacles-like structures ranges from tens to hundreds of nanometers. As shown in Fig. 1(b) and (c), when increasing the laser power to 1.48 W and 1.61 W, some irregular nanoporous structures with various shapes and sizes are generated near the center of the scanning line, and the tentacles-like structures could also be observed on the two sides of the scanning line. Furthermore, from the two sides to the center of the scanning line, the tentacles-like structures gradually evolve into nanoporous structures, which suggests that the nanoporous structures could be formed by the interconnection of tentacles-like structures. This could be explained by the Gaussian distribution of laser energy. The tentacles-like structures are formed on the two sides where the laser energy is low, and the nanoporous structures are generated near the central region where the laser energy is high. As shown in Fig. 1(d), when further increasing the laser power to 1.75 W, the nanoporous structures could still be formed, but the pore size decreases, which may be due to the continuous generation of tentacles-like structures with the increase in laser power. The experimental results in Fig. 1 indicate that the nanoporous structures are formed by the interconnection of tentacles-like structures, and their morphology strongly depends on the laser energy.

By single-line laser scanning, the nanoporous structures have been successfully fabricated on the Ti6Al4V surface. However, for practical engineering applications, large-area fabrication of the regular nanoporous structures is required. Therefore, the comparative experiments of multi-line laser scanning are further performed to investigate the formation and evolution of large-area nanoporous structures. Fig. 2 presents the SEM morphologies of the multi-line scanned regions obtained under various laser overlap rates. The applied laser power, scanning speed, and repetition frequency are 1.48 W, 10 mm/s, and 700 kHz, respectively. As shown in Fig. 2, when decreasing the laser overlap rate, the pore size and porosity of the nanoporous structures gradually increase. Additionally, when the laser overlap rate reduces to 64.3 %, some defects appear, leading to the irregularity of the nanoporous structures. This could be due to the unstable connection produced by the weakened generation of tentacles-like structures when a relatively low laser energy is presented in the junction of the adjacent laser scanning lines.

Fig. 3 presents the SEM morphologies of the multi-line scanned regions obtained under various scanning speeds. The applied laser power, repetition frequency, and overlap rate are 1.48 W, 700 kHz, and 76.6 %, respectively. Compared to the morphologies shown in

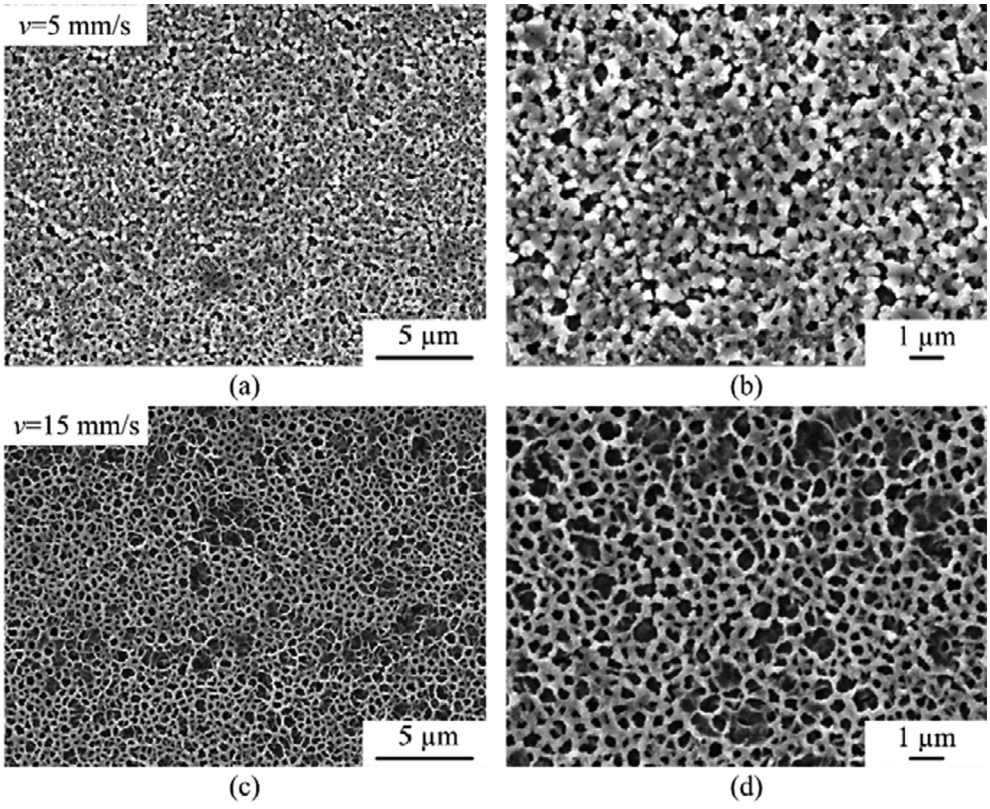

Fig. 3. SEM morphologies of the multi-line scanned regions obtained under various scanning speeds (P = 1.48 W, f = 700 kHz, r = 76.6 %): (a) v = 5 mm/s, (c) v = 15 mm/s. (b) and (d) are the local enlarged images of Fig. 3(a) and (c), respectively.

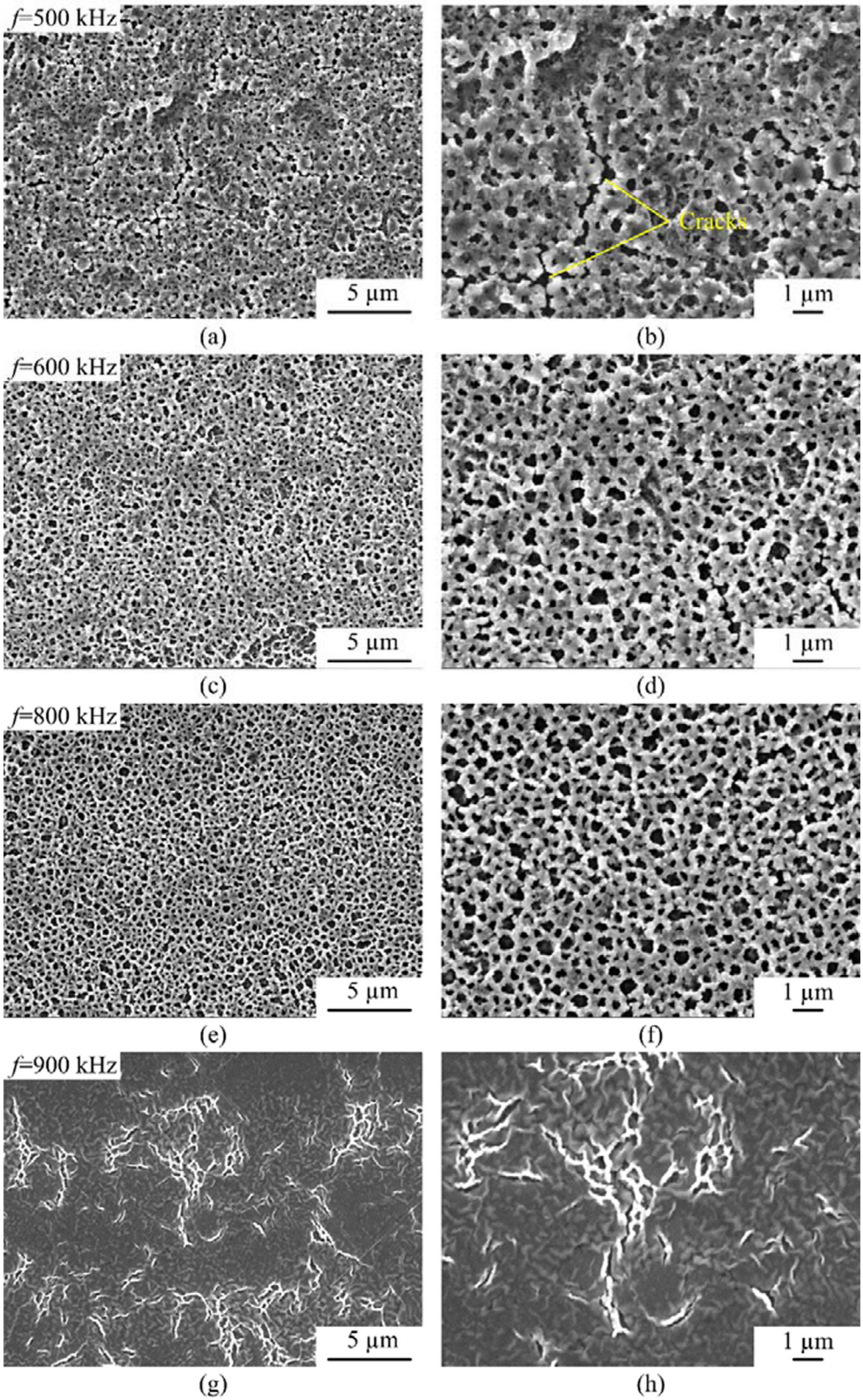

Fig. 4. SEM morphologies of the multi-line scanned regions obtained under various repetition frequencies (P = 1.48 W, v = 10 mm/s, r = 76.6 %): (a) 500 kHz, (c) 600 kHz, (e) 800 kHz, and (g) 900 kHz. (b), (d), (f), and (h) are the local enlarged images of Fig. 4(a), (c), (e), and (g), respectively.

Fig. 2(c) and (d), when the scanning speed reduces to 5 mm/s, the pore size and porosity of the nanoporous structures are drastically reduced in Fig. 3(a) and (b). However, as shown in Fig. 3(c) and (d), when increasing the scanning speed to 15 mm/s, the pore size and porosity of the nanoporous structures increase significantly. The above experimental results indicate that the scanning speed has a great influence on the surface features (pore size and porosity) of the nanoporous structures. Moreover, the nanoporous structures

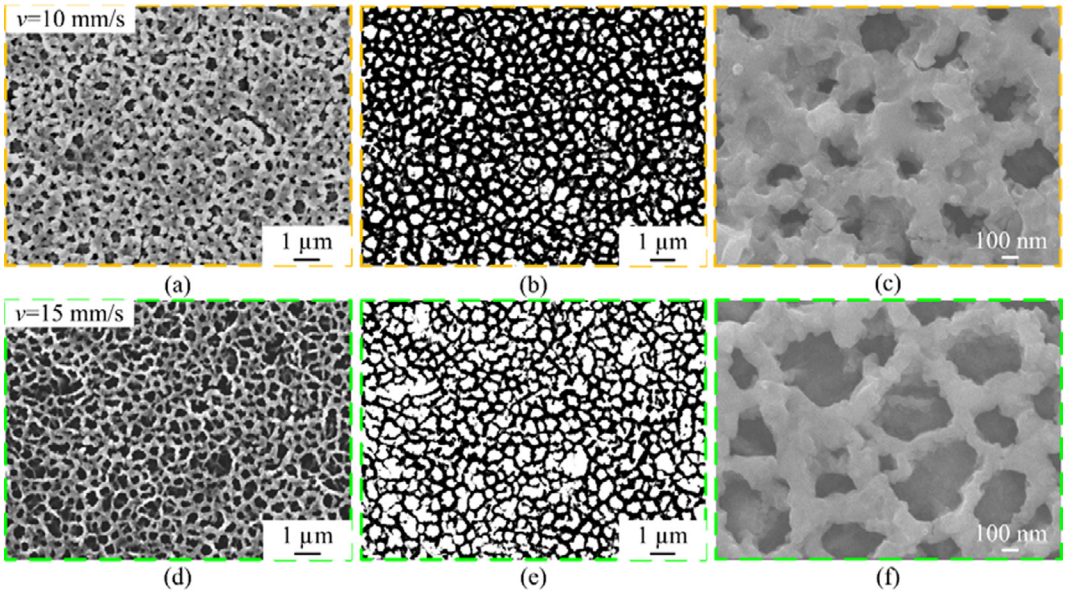

Fig. 5. SEM morphologies of two well-defined nanoporous structures with different porosities obtained under the applied laser parameters: (a) P = 1.48 W, v = 10 mm/s, r = 76.6 %, f = 700 kHz, and (d) P = 1.48 W, v = 15 mm/s, r = 76.6 %, f = 700 kHz. (b, e) and (c, f) show the binarized images and the local enlarged images of Fig. 5(a) and (d), respectively.

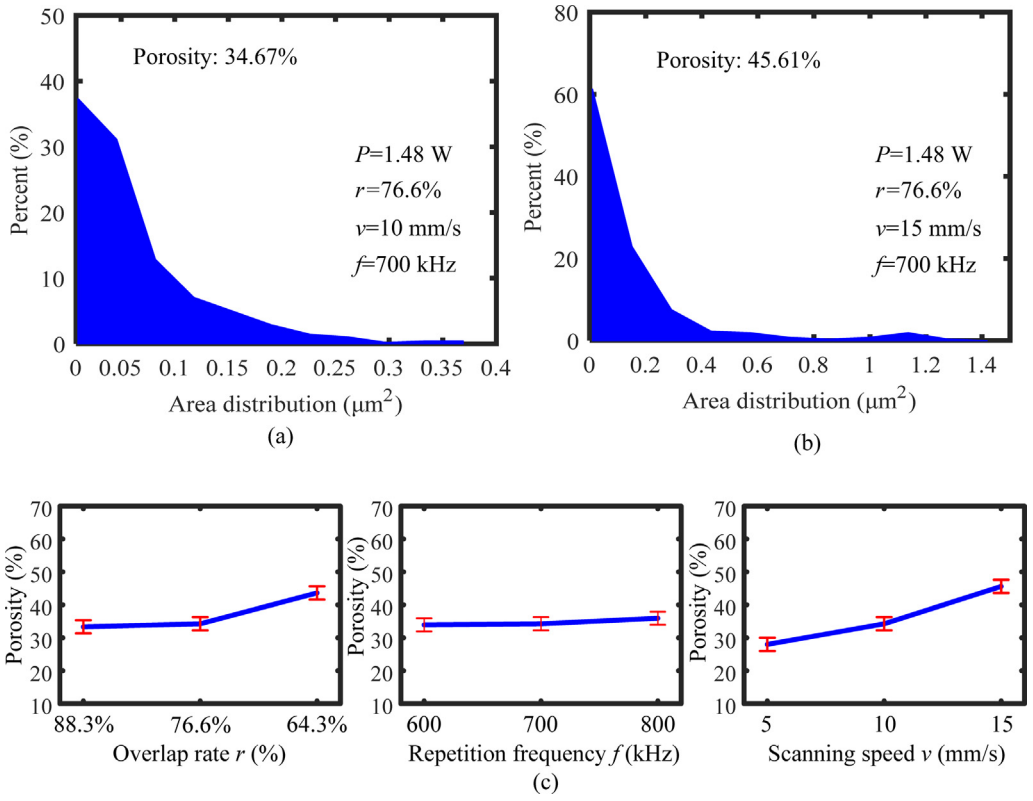

Fig. 6. (a) and (b) The percent of the pore area distribution of the nanoporous structures shown in Fig. 5(b) and (e). (c) The porosity varying with different laser parameters.

with similar surface features to those shown in Fig. 2(e) and (f) are formed in Fig. 3(c) and (d), but they have fewer defects. With the increase in the laser scanning speed, the laser energy is gradually weakened, but the laser overlap rate keeps constant. So, fewer defects appear at the junction of adjacent scanning lines compared to those shown in Fig. 2(e) and (f).

Fig. 4 presents the SEM morphologies of the multi-line scanned regions obtained under various repetition frequencies. The applied laser power, scanning speed, and overlap rate are 1.48 W, 10 mm/s, and 76.6 %, respectively. At a relatively low repetition frequency of 500 kHz, the nanoporous structures could not be clearly distinguished due to the relatively small pore size and porosity. Besides,

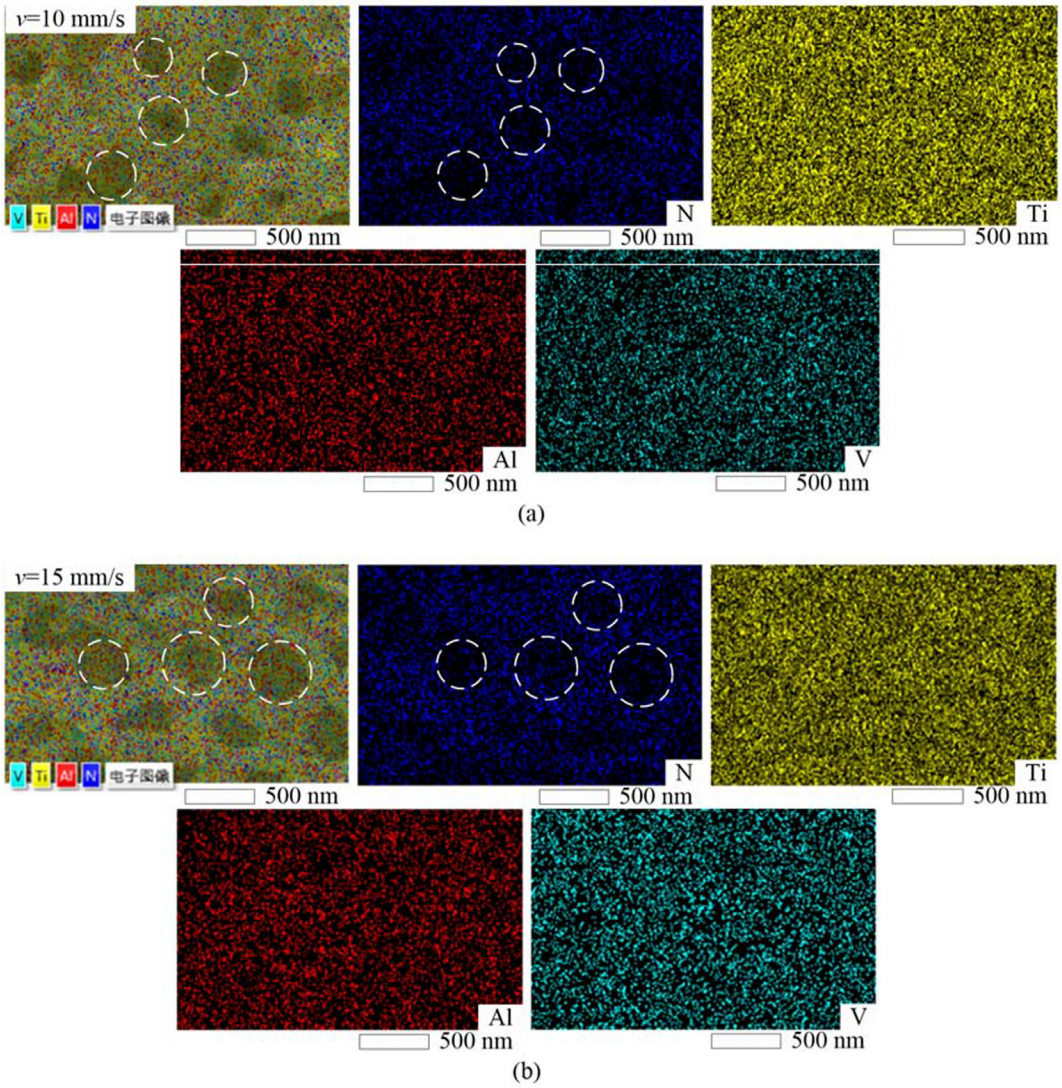

Fig. 7. SEM morphologies and the corresponding EDS element mappings obtained under various scanning speeds (P = 1.48 W, r = 76.6 %, f = 700 kHz): (a) 10 mm/s and (b) 15 mm/s.

some tiny cracks appear on the surface with the nanoporous structures. When increasing the repetition frequency to 600 ~ 800 kHz, well-defined nanoporous structures could be generated as shown in Fig. 4(c)-(f), and the porosity increases with the increase of repetition frequency. As shown in Fig. 4(g) and (h), when the repetition frequency reaches 900 kHz, the nanoporous structures are replaced by the tentacles-like structures. The difference in surface features of the nanoporous structures obtained under various repetition frequencies could be due to the change of pulse energy (E), which can be expressed as

$$E = \frac{P}{f} \tag{1}$$

where P is the average laser power. When the average laser power keeps unchanged, the pulse energy decreases with the increase of repetition frequency, leading to the difference in surface features of the nanoporous structures [31].

The above experimental results suggest that the porosity of nanoporous structures could be easily tuned by changing the laser parameters, and two well-defined nanoporous structures with different porosities are selected for further investigation. Fig. 5(a) and (b) present the corresponding SEM morphologies of nanoporous structures, one with a low porosity obtained under the laser parameters (P = 1.48 W, v = 10 mm/s, r = 76.6 %, f = 700 kHz) and the other with a high porosity obtained under the laser parameters (P = 1.48 W, v = 15 mm/s, r = 76.6 %, f = 700 kHz). From the enlarged images in Fig. 5(c) and (f), the pore size of two typical nanoporous structures is quite different, which may be the main reason for the change in porosity. To facilitate quantitative characterization of nanoporous structures, the SEM images are converted into binarized images by the ImageJ software, and the results are presented in Fig. 5(b) and (e).

By analyzing the binarized images in Fig. 5(b) and (e), Fig. 6(a) and (b) present the percent of the pore area distribution of the nanoporous structures. It is clearly seen that the pore area distribution of nanoporous structures with low porosity (34.67 %) is mainly concentrated in 0 ~ 0.1 μm^2; while for the nanoporous structures with high porosity (45.61 %), the pore area distribution is mainly concentrated in 0 ~ 0.3 μm^2. This further indicates that the change in porosity is mainly related to the pore size. Fig. 6(c) shows the porosity varying with the laser overlap rate, repetition frequency, and scanning speed. Among these three laser parameters, the scanning speed has the most significant effect on the porosity of nanoporous structures, followed by the overlap rate. In the range of 600 ~ 800 kHz, the effect of repetition frequency on porosity is very weak.

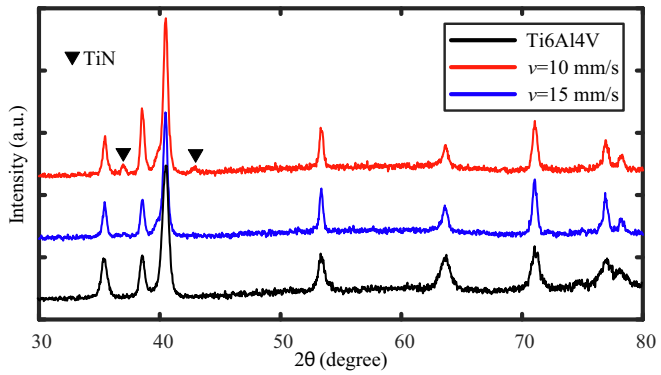

Fig. 8. XRD patterns of the Ti6Al4V surface and the laser irradiated surfaces obtained under various scanning speeds (P = 1.48 W, r = 76.6 %, f = 700 kHz).

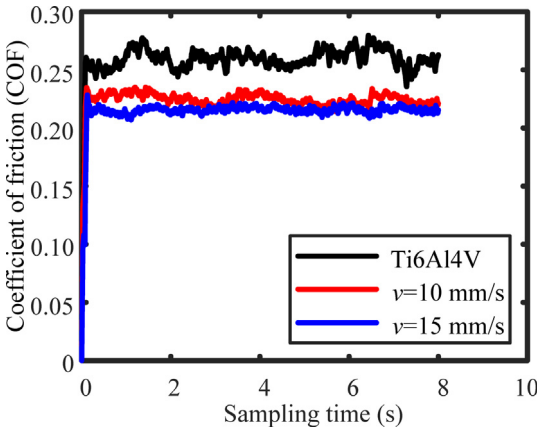

Fig. 10. The COF curves of the Ti6Al4V surface, as well as the surfaces with nanoporous structures obtained under different laser scanning speeds (P = 1.48 W, r = 76.6 %, f = 700 kHz): v = 10 mm/s and v = 15 mm/s. The scratch load is kept to 100 mN.

3.2. Chemical composition of the nanoporous structures

To verify whether the formation of nanoporous structures is related to the surface chemistry, the EDS mapping and XRD analysis are performed for investigating the chemical composition after laser irradiation. Fig. 7 presents the SEM morphologies and the corresponding EDS element mappings obtained under various scanning speeds. It is noted that element N is newly introduced into the surface with nanoporous structures after laser irradiation. Furthermore, the distribution of element N matches the location of the nanoporous structures, which suggests that the element N is associated with the formation of nanoporous structures. However, the distribution of elements Ti, Al, and V is uniform for nanoporous structures with different porosities. The results of XRD analysis are shown in Fig. 8. When the scanning speed is 15 mm/s, the irradiated surface exhibits almost the same XRD pattern as the Ti6Al4V surface. When the scanning speed reduces to 10 mm/s, the slight crystalline peaks of the TiN phase could be identified in the XRD pattern of the irradiated surface, indicating the generation of the TiN phase.

By the experimental results and analysis, the onset of nanoporous structures is essentially initiated by the interconnection of tentacles-like structures. And these irregular tentacles-like struc-

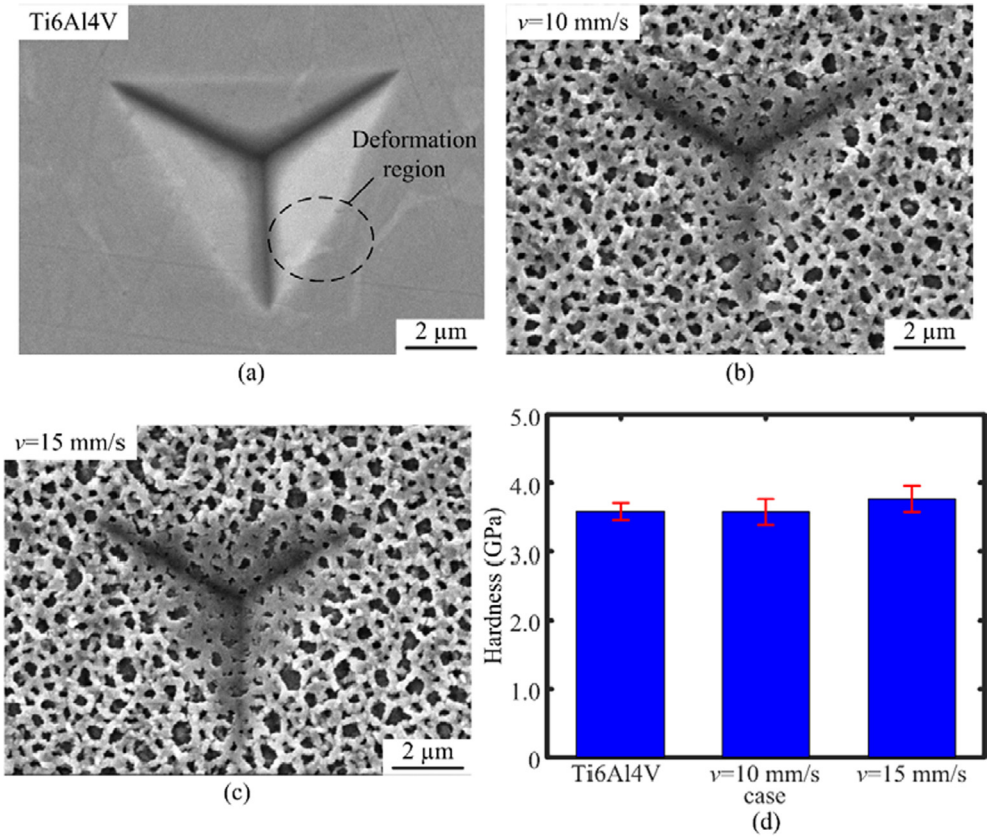

Fig. 9. SEM morphologies of the residual indents on (a) the Ti6Al4V surface, as well as the surfaces with nanoporous structures obtained under different laser scanning speeds (P = 1.48 W, r = 76.6 %, f = 700 kHz): (b) v = 10 mm/s and (c) v = 15 mm/s. (d) The distribution of surface hardness corresponding to the residual indents shown in Fig. 9(a), (b), and (c). The indentation load is kept to 100 mN.

tures are also a kind of nanostructures, and their morphology is affected by laser parameters. According to some previous studies [33–35], the generation of nanostructures relies on the spontaneous behavior during laser-material interaction, which is generally explained by a self-assembly mechanism involving Marangoni instability and rarefaction wave in shallow melting layer. On the other hand, similar nanoporous structures are not observed in the comparative experiments under argon and ambient atmospheres. Therefore, the introduction of the element N may induce the self-assembly behavior of the irradiated surface, leading to the generation of tentacles-like structures, which subsequently evolve into the nanoporous structures.

3.3. Performance characterization of the nanoporous structures

According to the above experimental results, the micromechanical properties and wettability of two typical nanoporous structures with different porosities are further characterized. The SEM morphologies of residual indents obtained on the Ti6Al4V surface and the surfaces with nanoporous structures are presented in Fig. 9(a), (b), and (c), respectively. The small deformation region could be observed around the residual indent of the Ti6Al4V surface, and the residual indents of nanoporous structures present a uniform topographical feature. The corresponding distribution of surface hardness is illustrated in Fig. 9(d). In general, the surface hardness of bulk material would decrease due to the increase of surface porosity, but for the surface with nanoporous structures here, the surface hardness is almost the same as that of the original Ti6Al4V surface (~3.6 GPa). On the one hand, EDS and XRD results demonstrate that laser nitriding (i.e. the introduction of element N and the formation of hard phase TiN) has occurred, which could weaken the reduction of surface hardness induced by porous structures. On the other hand, as the nanoporous structures have unique nanoscale features, they would possess some unique mechanical properties due to the size effect [36–39]. This may also lead to the increase of surface hardness.

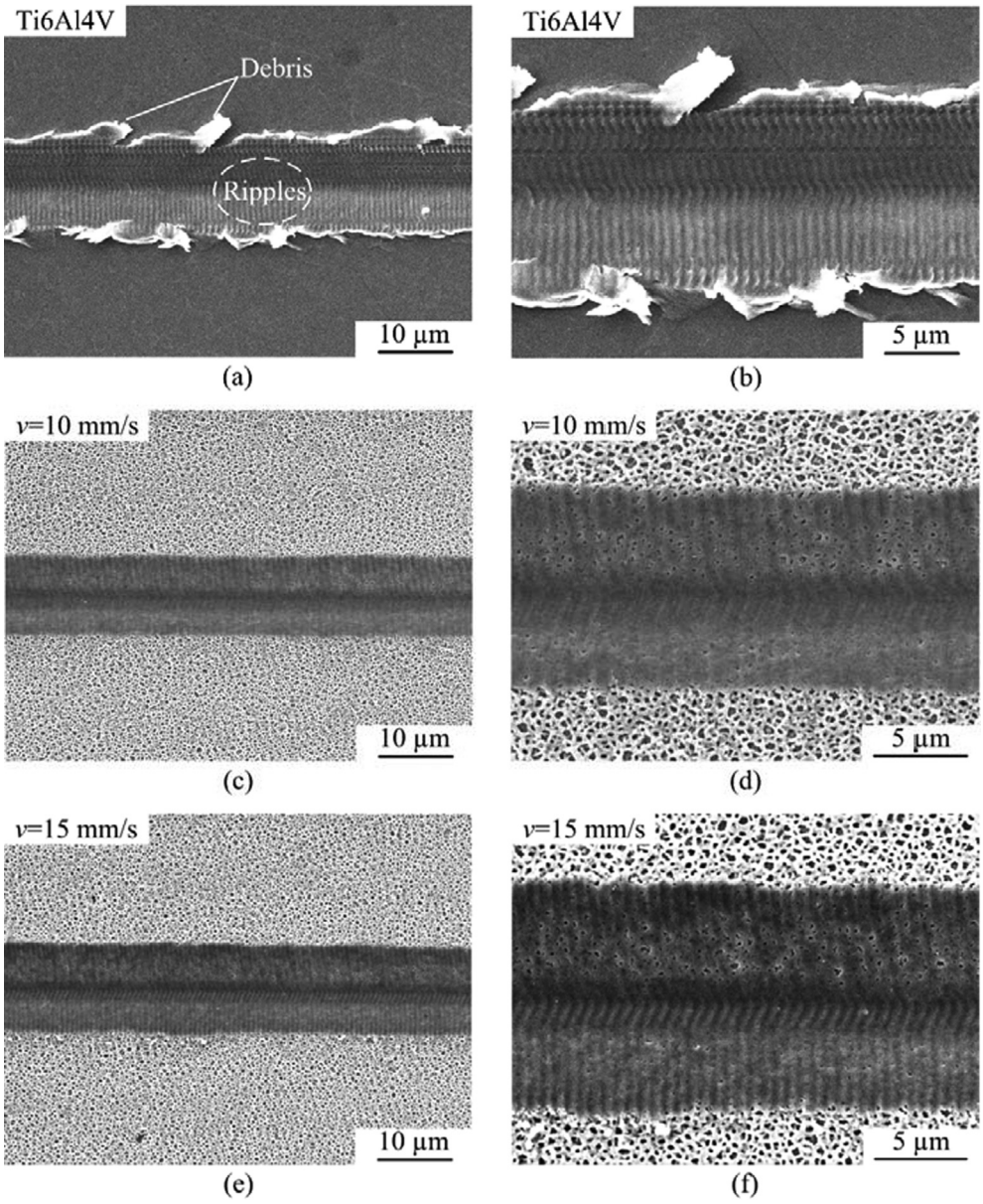

Fig. 11. The SEM morphologies of the residual scratches obtained on (a) and (b) the original Ti6Al4V surface, as well as the surfaces with nanoporous structures obtained under different laser scanning speeds (P = 1.48 W, r = 76.6 %, f = 700 kHz): (c) and (d) v = 10 mm/s, (e) and (f) v = 15 mm/s. The scratch load is kept to 100 mN.

To investigate the effects of nanoporous structures on tribological performance, scratch tests are performed on the Ti6Al4V surface as well as the surfaces with nanoporous structures. The coefficient of friction (COF), defined by the ratio of the tangential force to the normal force, is used to evaluate the tribological performance of the surface. Fig. 10 shows the COF curves. It is clearly seen that the COFs of the surfaces with nanoporous structures are smaller than that of the Ti6Al4V surface. Furthermore, for the nanoporous structures with different porosities, their COFs are almost the same, which may be related to the similar surface morphologies and surface hardness. The corresponding SEM morphologies of the residual scratches are presented in Fig. 11. For the original Ti6Al4V surface as shown in Fig. 11(a) and (b), the regular ripples could be observed on the inner surface of the residual scratch, and some debris appear around the two sides of the residual scratch. The inner ripples are caused by the intrinsic backward motion of the stick–slip piezoelectric actuator in the scratch instrument [40]. The debris around scratches is formed by the plastic deformation of Ti6Al4V material due to the extrusion during the scratching [41,42]. Being quite different from these features, for the surfaces with nanoporous structures, no debris appears around the two sides of residual scratches, and only slight ripples could be observed on the inner surface. This indicates that the nanoporous structures could improve the tribological characteristics of the Ti6Al4V surface. The experimental results show that under the same scratch load, the tangential force of the surface with nanoporous structures decreases, weakening the plastic deformation of Ti6Al4V material. Besides, some previous studies [43,44] showed that the nanoporous structures would exhibit good ductility in the micro-state and possess excellent strength due to the unique stress distribution caused by the circular pore shape under compression. As a result, the surfaces with nanoporous structures exhibit better tribological characteristics during scratching, with inhibited debris and ripples.

Fig. 12(a), (b), and (c) present the three-dimensional (3D) topographies of the residual scratches corresponding to Fig. 11. The profiles of the cross-sections are illustrated in Fig. 12(d). For the surfaces with nanoporous structures, the depth of the residual scratches and the height of accumulation around the two sides are obviously smaller than those of the original Ti6Al4V surface. The difference in depth and height is 0.17 μm and 0.34 μm, respectively. This further proves the positive effect of nanoporous structures during scratching. The EDS mappings of the residual scratches corresponding to Fig. 11 are presented in Fig. 13. The elemental content of the nanoporous material before and after scratching is listed in Table 2. For the surface of nanoporous material obtained under different scanning speeds, the content of all elements is not changed before and after scratching, which indicates that the nanoporous structures are destroyed but not removed under the scratch load of 100 mN.

Some previous studies [45,46] demonstrated that surface textures could significantly tune the wettability of the material surface. Therefore, the contact angles of the surface with nanoporous structures (P = 1.48 W, v = 15 mm/s, r = 76.6 %, f = 700 kHz) are measured for evaluating the wettability, and the corresponding experimental results are shown in Fig. 14. The con-

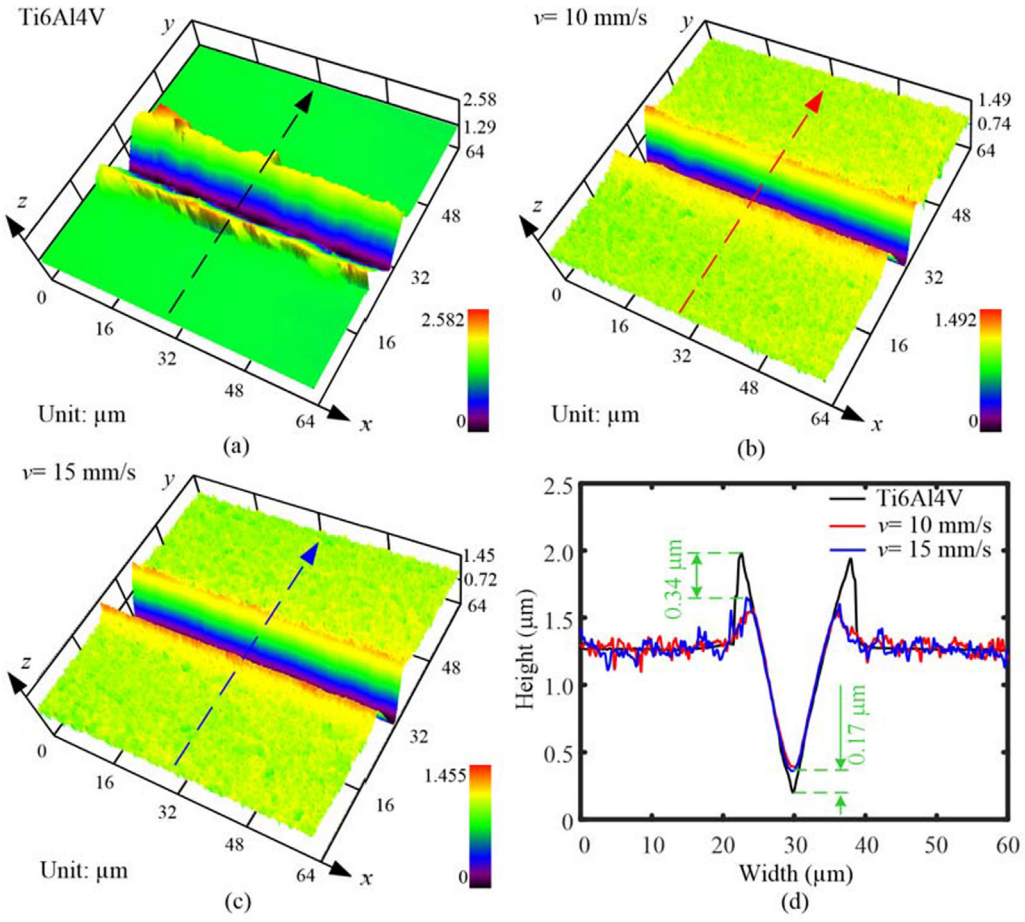

Fig. 12. 3D topographies of the residual scratches obtained on (a) the Ti6Al4V surface and the surfaces with nanoporous structures obtained under different laser scanning speeds (P = 1.48 W, r = 76.6 %, f = 700 kHz): (b) v = 10 mm/s and (c) v = 15 mm/s. (d) Profiles of the cross-sections marked in Fig. 12(a)-(c). The scratch load is kept to 100 mN.

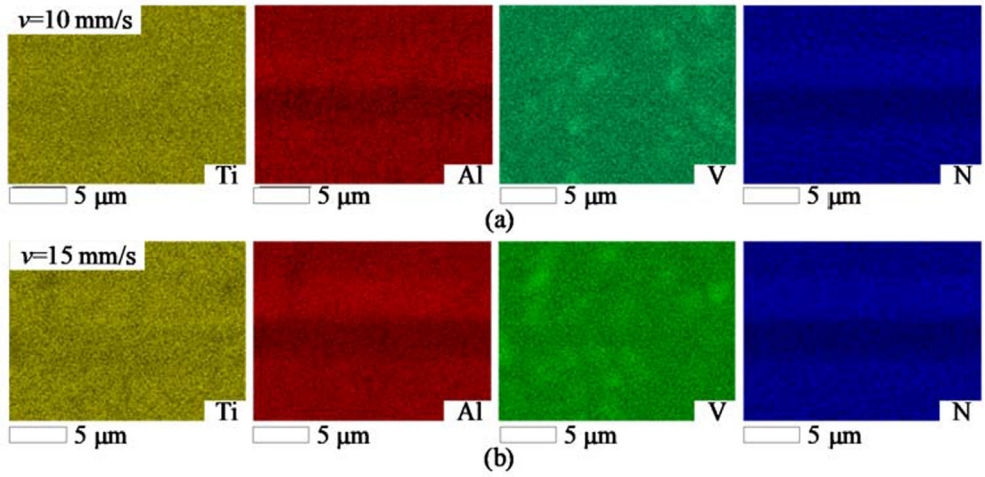

Fig. 13. The EDS mappings of the residual scratches corresponding to (a) Fig. 11(d), and (b) Fig. 11(f).

Table 2
Elemental content of the nanoporous material before and after scratching in Fig. 13.

Laser parameter	Region	Ti (at.%)	Al (at.%)	V (at.%)	N (at.%)
v = 10 mm/s	before scratching	60.7 ± 0.20	6.4 ± 0.17	2.4 ± 0.05	30.5 ± 0.05
	after scratching	60.5 ± 0.18	6.5 ± 0.18	2.5 ± 0.07	30.6 ± 0.21
v = 15 mm/s	before scratching	60.6 ± 0.20	6.6 ± 0.17	2.4 ± 0.05	30.4 ± 0.05
	after scratching	60.0 ± 0.18	6.6 ± 0.18	2.5 ± 0.07	30.9 ± 0.21

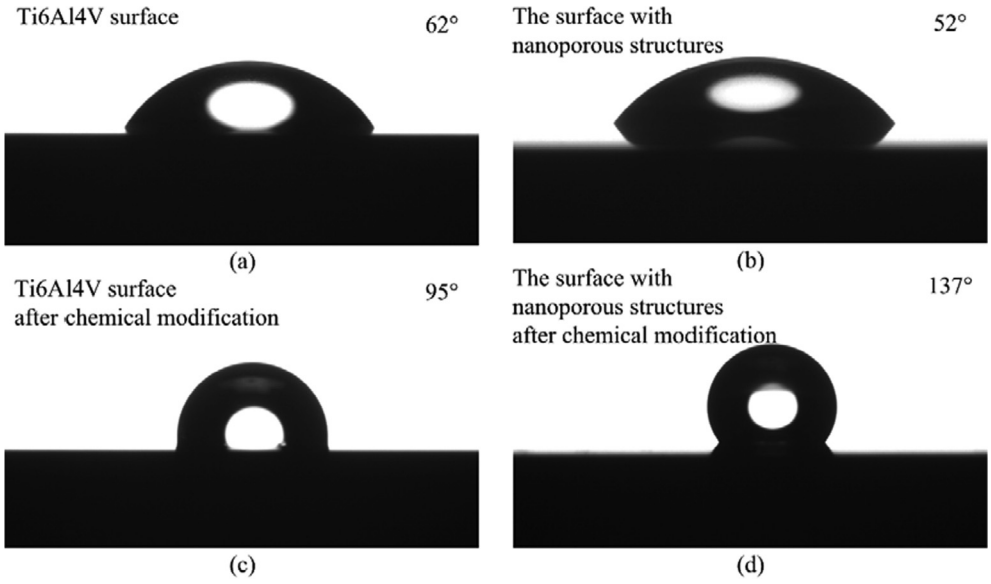

Fig. 14. Contact angles of (a) the polished Ti6Al4V surface, (b) the surface with nanoporous structures, (c) the polished Ti6Al4V surface after chemical modification, and (d) the surface with nanoporous structures after chemical modification.

tact angle of the polished Ti6Al4V surface is about 62°, and the surface with nanoporous structures shows a contact angle of 52°, indicating that the nanoporous structures slightly increase the hydrophilicity. After chemical modification, the contact angles of the Ti6Al4V surface and the surface with nanoporous structures are 95° and 137°, respectively. Compared to the Ti6Al4V surface, the hydrophobicity of the surface with nanoporous structures after chemical modification is significantly increased. It should be pointed out that when the porosity is changed in the range of 35 % to 45 %, the surface with nanoporous structures shows the almost same wetting behavior due to the similar morphological features.

4. Conclusions

In summary, by nanosecond pulse laser irradiation in nitrogen atmosphere, the formation of nanoporous structures on the

Ti6Al4V surface was observed. The effects of laser irradiation parameters on their formation and evolution were investigated in detail, followed by characterizing their micro-mechanical properties and wettability. By experiments and analysis, the following conclusions could be obtained.

(1) By nanosecond pulse laser irradiation in nitrogen atmosphere, the well-defined nanoporous structures could be produced on the Ti6Al4V surface, and their porosity can be easily tuned by changing the laser parameters.

(2) Compared to the original Ti6Al4V surface, the surfaces with nanoporous structures exhibited similar surface hardness but superior tribological performance, which was related to the introduction of the TiN phase as well as the intrinsic properties of nanoscale structures.

(3) The formed nanoporous structures could tune the wettability of the Ti6Al4V surface.

This study provides an alternative method for fabricating nanoporous structures on the Ti6Al4V surface via laser processing. This method has the advantages of simple equipment requirements, easy operation, good repeatability, and no pollution, which is expected to be used for pilot scale-up production of nanoporous materials on the titanium alloy.

Data availability

Data will be made available on request.

Declaration of Competing Interest

The authors declare that they have no known competing financial interests or personal relationships that could have appeared to influence the work reported in this paper.

Acknowledgements

This work was supported by the Jilin Provincial Natural Science Foundation (Grant No. 20220101198JC), the National Natural Science Foundation of China (Grant No. 52075221), and the Fundamental Research Funds for the Central Universities (2020-2022).

Data availability

The raw/processed data required to reproduce these findings cannot be shared at this time due to technical or time limitations. After acceptance, the raw/processed data can be available from the corresponding author upon reasonable request.

References

[1] A. Albanese, P.S. Tang, W.C.W. Chan, The effect of nanoparticle size, shape, and surface chemistry on biological systems, Annu. Rev. Biomed. Eng. 14 (1) (2012) 1–16.
[2] M. Goyal, M. Singh, Size and shape dependence of optical properties of nanostructures, Appl. Phys. A 126 (3) (2020).
[3] N. Baig, I. Kammakakam, W. Falath, Nanomaterials: a review of synthesis methods, properties, recent progress, and challenges, Mater. Adv. 2 (6) (2021) 1821–1871.
[4] J.T. Zhang, C.M. Li, Nanoporous metals: fabrication strategies and advanced electrochemical applications in catalysis, sensing and energy systems, Chem. Soc. Rev. 41 (21) (2012) 7016–7031.
[5] Y. Li, H.X. Cao, J.H. Yu, Toward a new era of designed synthesis of nanoporous zeolitic materials, ACS Nano 12 (5) (2018) 4096–4104.
[6] C. Toccafondi, R. La Rocca, A. Scarpellini, M. Salerno, G. Das, S. Dante, Thin nanoporous alumina-based sers platform for single cell sensing, Appl. Surf. Sci. 351 (2015) 738–745.
[7] J.T. Li, G.C. Zhang, H.M. Zhang, X. Fan, L.S. Zhou, Z.Y. Shang, X.T. Shi, Electrical conductivity and electromagnetic interference shielding of epoxy nanocomposite foams containing functionalized multi-wall carbon nanotubes, Appl. Surf. Sci. 428 (2018) 7–16.
[8] X.Y. Lang, A. Hirata, T. Fujita, M.W. Chen, Nanoporous metal/oxide hybrid electrodes for electrochemical supercapacitors, Nat. Nanotechnol. 6 (4) (2011) 232–236.
[9] E.W. Andrews, G. Gioux, P. Onck, L.J. Gibson, Size effects in ductile cellular solids. Part Ii: experimental results, Int. J. Mech. Sci. 43 (3) (2001) 701–713.
[10] Z.J. Yang, Z.Y. Xie, H. Liu, F. Yan, H.X. Ju, Streptavidin-functionalized three-dimensional ordered nanoporous silica film for highly efficient chemiluminescent immunosensing, Adv. Funct. Mater. 18 (24) (2008) 3991–3998.
[11] A. Mehmood, G. Ali, B. Koyuturk, J. Pampel, K.Y. Chung, T.P. Fellinger, Nanoporous nitrogen doped carbons with enhanced capacity for sodium ion battery anodes, Energy Storage Mater. 28 (2020) 101–111.
[12] A. Ghosh, F. Vallam Thodi, S. Sengupta, S. Kannan, L. Krishnan, E. Bhattacharya, Effective clearance of uremic toxins using functionalised silicon nanoporous membranes, Biomed. Microdevices 23 (1) (2021) 4.
[13] W. Wei, R. Kirchgeorg, K. Lee, S. So, P. Schmuki, Nitrates: A New Class Of Electrolytes for the Rapid Anodic Growth of Self-Ordered Oxide Nanopore Layers on Ti And Ta, Phys. Status. Solidi-R 5 (10–11) (2011) 394–396.
[14] M. Tiemann, C. Weinberger, Selective modification of hierarchical pores and surfaces in nanoporous materials, Adv. Mater. Interfaces 8 (4) (2021) 2001153.
[15] R.S. Williamson, J. Disegi, J.A. Griggs, M.D. Roach, Nanopore Formation on yhe Surface Oxide of Commercially Pure Titanium Grade 4 Using a Pulsed Anodization Method in Sulfuric Acid, J. Mater. Sci. Mater. Med. 24 (10) (2013) 2327–2335.
[16] P. Peng, H. Sun, A.P. Gerlich, W. Guo, Y. Zhu, L. Liu, G.S. Zou, C.V. Singh, N. Zhou, Near-ideal compressive strength of nanoporous silver composed of nanowires, Acta Mater. 173 (2019) 163–173.
[17] Z. Lu, C. Li, J. Han, F. Zhang, P. Liu, H. Wang, Z. Wang, C. Cheng, L. Chen, A. Hirata, T. Fujita, J. Erlebacher, M. Chen, Three-dimensional bicontinuous nanoporous materials by vapor phase dealloying, Nat. Commun. 9 (1) (2018) 276.
[18] M. Heidari, J. Yan, Material removal mechanism and surface integrity in ultraprecision cutting of porous titanium, Precis. Eng. 52 (2018) 356–369.
[19] Y.T. Yao, Y. Yang, Q. Ye, S.S. Cao, X.P. Zhang, K. Zhao, Y. Jian, Effects of Pore size and porosity on cytocompatibility and osteogenic differentiation of porous titanium, J. Mater. Sci. Mater. Med. 32 (6) (2021) 72.
[20] S. Zhang, Q. Wei, L. Cheng, S. Li, Y. Shi, Effects of scan line spacing on pore characteristics and mechanical properties of porous Ti6Al4V implants fabricated by selective laser melting, Mater. Des. 63 (2014) 185–193.
[21] Y. Su, S. Komasa, T. Sekino, H. Nishizaki, J. Okazaki, Nanostructured Ti6Al4V alloy fabricated using modified alkali-heat treatment: characterization and cell adhesion, Mater. Sci. Eng. C Mater. Biol. Appl. 59 (2016) 617–623.
[22] J. Xia, Y. Yuan, H. Wu, Y. Huang, D.A. Weitz, Decoupling the effects of nanopore size and surface roughness on the attachment, spreading and differentiation of bone marrow-derived stem cells, Biomaterials 248 (2020) 120014.
[23] M. Ferrà-Cañellas, M. Llopis-Grimalt, M. Monjo, J. Ramis, Tuning nanopore diameter of titanium surfaces to improve human gingival fibroblast response, Int. J. Mol. Sci. 19 (10) (2018) 2881.
[24] D.-S. Shim, J.-Y. Seo, Fabrication of porous metals layered by laser-assisted melting of sprayed Ti6al4v powder and foaming agent mixture, Mater. Lett. 219 (2018) 243–246.
[25] S.A. Yavari, R. Wauthle, J. van der Stok, A.C. Riemslag, M. Janssen, M. Mulier, J.P. Kruth, J. Schrooten, H. Weinans, A.A. Zadpoor, Fatigue behavior of porous biomaterials manufactured using selective laser melting, Mater. Sci. Eng. C Mater. Biol. Appl. 33 (8) (2013) 4849–4858.
[26] T. Dikici, A.H. Guzelaydin, M. Toparli, Formation and characterisation of nanoporous TiO2 layers on microroughened titanium surfaces by electrochemical anodisation, Micro & Nano Lett. 9 (2) (2014) 144–148.
[27] H. Tao, G.-J. Fang, W.-J. Ke, W. Zeng, J. Wang, In-Situ Synthesis of TiO2 Network Nanoporous Structure on Ti Wire Substrate and Its Application in Fiber Dye Sensitized Solar Cells, J. Power Sources 245 (2014) 59–65.
[28] C. Wang, H. Huang, Y. Qian, Z. Zhang, J. Yan, One-Step Fabrication of Regular Hierarchical Micro/Nano-Structures on Glassy Carbon by Nanosecond Pulsed Laser Irradiation, J. Manuf. Process 62 (2021) 108–118.
[29] H. Huang, N. Jun, M. Jiang, M. Ryoko, J. Yan, Nanosecond Pulsed Laser Irradiation Induced Hierarchical Micro/Nanostructures on Zr-Based Metallic Glass Substrate, Mater. Des. 109 (2016) 153–161.
[30] G. Luo, D.i. Wu, Y.u. Zhou, Y. Hu, Z. Yao, Laser printing of large-scale metal micro/nanoparticle array: Deposition behavior and microstructure, Int. J. Mach. Tool. Manu. 173 (2022).
[31] C. Wang, H. Huang, Y. Qian, Z. Zhang, W. Huang, J. Yan, Nitrogen assisted formation of large-area ripples on Ti6Al4V surface by nanosecond pulse laser irradiation, Precis. Eng. 73 (2022) 244–256.
[32] Y. Qian, H. Huang, C. Wang, P. Yu, J. Xu, Z. Zhang, Formation of Leaf-Shaped Microstructure on Zr-Based Metallic Glass via Nanosecond Pulsed Laser Irradiation, J. Manuf. Process 72 (2021) 61–70.
[33] A. Abou Saleh, A. Rudenko, S. Reynaud, F. Pigeon, F. Garrelie, J.P. Colombier, Sub-100 Nm 2D Nanopatterning on A Large Scale by Ultrafast Laser Energy Regulation, Nanoscale 12 (12) (2020) 6609–6616.
[34] J. Reif, O. Varlamova, F. Costache, Femtosecond Laser Induced Nanostructure Formation: Self-Organization Control Parameters, Appl. Phys. A 92 (4) (2008) 1019–1024.
[35] M. Prudent, F. Bourquard, A. Borroto, J.-F. Pierson, F. Garrelie, J.-P. Colombier, Initial Morphology and Feedback Effects on Laser-Induced Periodic Nanostructuring of Thin-Film Metallic Glasses, Nanomaterials (Basel) 11 (5) (2021) 1076.

[36] Z. Li, X. Lu, Nanoindentation for mechanical behaviour characterization of nanoporous silver fabricated through dealloying, B, Mater. Sci. 44 (2) (2021).
[37] A.M. Hodge, J.R. Hayes, J.A. Caro, J. Biener, A.V. Hamza, Characterization and mechanical behavior of nanoporous gold, Adv. Eng. Mater. 8 (9) (2006) 853–857.
[38] J. Biener, A.M. Hodge, J.R. Hayes, C.A. Volkert, L.A. Zepeda-Ruiz, A.V. Hamza, F.F. Abraham, Size effects on the mechanical behavior of nanoporous Au, Nano Lett. 6 (10) (2006) 2379–2382.
[39] W. Yang, Z.P. Luo, W.K. Bao, H. Xie, Z.S. You, H.J. Jin, Light, strong, and stable nanoporous aluminum with native oxide shell, Sci. Adv. 7 (28) (2021).
[40] Z. Yang, X. Zhou, H. Huang, J. Dong, Z. Fan, H. Zhao, On the suppression of the backward motion of a piezo-driven precision positioning platform designed by the parasitic motion principle, IEEE T. Ind. Electron. 67 (5) (2020) 3870–3878.
[41] S. Durdu, M. Sancak, E. Yalcin, M. Usta, E. Akagunduz, A. Altinkok, Surface Characterization of TiO2 Nanotube Arrays Produced on Ti6Al4V Alloy by Anodic Oxidation, Surf. Coat. Tech. 428 (2021) 127903.
[42] K. Palaniappan, M. Sundararaman, H. Murthy, R. Jeyaraam, B.C. Rao, Influence of workpiece texture and strain hardening on chip formation during machining of Ti–6Al–4V alloy, Int. J. Mach. Tool. Manu. 173 (2022) 103849.
[43] Z. Li, X. Lu, Q. Wang, S. Zhang, Effect of nanoindentation depth and ligament size on mechanical properties of nanoporous silver, Micro & Nano Lett. 13 (4) (2018) 461–464.
[44] M. Nasr Esfahani, M. Jabbari, Molecular dynamics simulations of deformation mechanisms in the mechanical response of nanoporous gold, Materials 13 (9) (2020) 2071.
[45] H. Chen, P. Zhang, L. Zhang, H. Liu, Y. Jiang, D. Zhang, Z. Han, L. Jiang, Continuous directional water transport on the peristome surface of nepenthes Alata, Nature 532 (7597) (2016) 85–89.
[46] D. Wang, Q. Sun, M.J. Hokkanen, C. Zhang, F.Y. Lin, Q. Liu, S.P. Zhu, T. Zhou, Q. Chang, B. He, Q. Zhou, L. Chen, Z. Wang, R.H.A. Ras, X. Deng, Design of robust superhydrophobic surfaces, Nature 582 (7810) (2020) 55–59.